Long-Term Colloidal and Chemical Stability in Aqueous Media of NaYF₄-Type Upconversion Nanoparticles Modified by Ligand-Exchange

*Sandy F. Himmelstoß and Thomas Hirsch**

Surface capping is an essential component of nanoparticles as it provides access to their outstanding properties in the real world. Upconversion nanoparticles are predominantly interesting for use in biological environments, due to their excellent optical properties such as the conversion of near-infrared excitation light into emissions in the visible or UV range of the spectrum, high photostability, and the absence of any intermittence. One of the most efficient upconversion nanoparticles, consisting of lanthanide doped NaYF₄, suffers from limited stability in aqueous media. This study investigates a set of five types of surface coatings, ranging from small ligands to polymers of different charge and different coordinating groups, on monodisperse 28 ± 0.9 nm sized NaYF₄(Yb,Er) nanoparticles modified by a two-step ligand exchange mediated by NOBF₄. Information on the long-term chemical and colloidal stability for highly diluted aqueous dispersions of these particles is acquired by transmission electron microscopy, dynamic light scattering, and luminescence spectroscopy. The findings are of importance for the development of probes and labels based on upconversion nanoparticles for biological applications.

1. Introduction

Upconversion nanoparticles (UCNPs) established in the last years as versatile luminescent probes due to intense progress in the synthesis enabling complex particle architectures of controlled dimensions.[1–3] As a consequence, also the photophysical principles of photon upconversion, including luminescence efficiency affected by surface quenching and passivation processes have been excessively studied.[4–6] The absence of any background fluorescence in biological media due to the unique optical properties of the upconversion of low energy photons in the near-infrared (NIR) region into high energy emissions in the visible or UV[7] makes this material promising for biological applications. But this comes with several challenges like chemical and colloidal stability in aqueous media or the controlled functionalization

by a defined number of receptor molecules.[8–10] Most upconversion nanoparticles described in literature are consisting of a NaYF₄ host lattice as this materials has a preferable low phonon-energy[11] (≈ 300 cm⁻¹) compared to other host materials like fluorides (LiYbF₄, ≈ 460 cm⁻¹[12]), oxides (Y₂O₃, ≈ 591 cm⁻¹[13]), or vanadates (YVO₃, ≈ 890 cm⁻¹[14]). Therefore, it is not surprising that this host material together with Yb³⁺ and Er³⁺ has been used to design the most efficient upconversion nanoparticles.[1,15] However, the synthesis of those nanoparticles is often based on thermal decomposition of lanthanide oleates[16] or acetates[1] in high boiling organic solvents, ending up with a hydrophobic surface ligand (e.g., oleic acid).[17] To make the particles accessible for biological applications, different surface engineering strategies have been developed to render the particles water dispersible.[18,19]

Thereby, the simplest method is the removal of the surface ligands assisted by an acid.[20] Alternatively, the removal of the ligands is performed before the addition of a stabilizing agent like citrate. The oleic acid can be removed via the acidic form of the surface ligand (e.g., citric acid[21]) or by NOBF₄.[22] Other techniques not requiring the removal of the oleic acid are based on the interaction of amphiphilic molecules and hydrophobic capping agents. As reported by the group of Parak[23] a comb-like polymer consisting of a poly(maleic anhydride) backbone with a modified hydrophobic chain can be used for the successful transfer of colloidal nanoparticles into a hydrophilic environment. During this process, also polymer micelles with no UCNPs inside are generated.[24] This is attributed by the intention to ensure a complete coating of the UCNPs by using an excess of the amphiphilic polymer. Such empty micelles cannot be separated easily from the modified particles and may affect certain applications. For instance, when the polymer is labeled with additional dyes, those empty structures may falsify the results. Another popular strategy is the coating of the particles with silica. Such silica shells can be prepared by the Stöber method, which involves the controlled hydrolysis and condensation of siloxane monomers.[25] However, particles with silica coating often show poor temporal stability under physiological conditions in aqueous dispersions of high salt concentration or in the presence of highly charged ions like phosphates.[18]

In many studies, the impact of the surface chemistry is neglected or only tackled with a minor interest in terms of

Dr. S. F. Himmelstoß, Dr. T. Hirsch
University of Regensburg
Universitätsstraße 31, 93053 Regensburg, Germany
E-mail: thomas.hirsch@ur.de

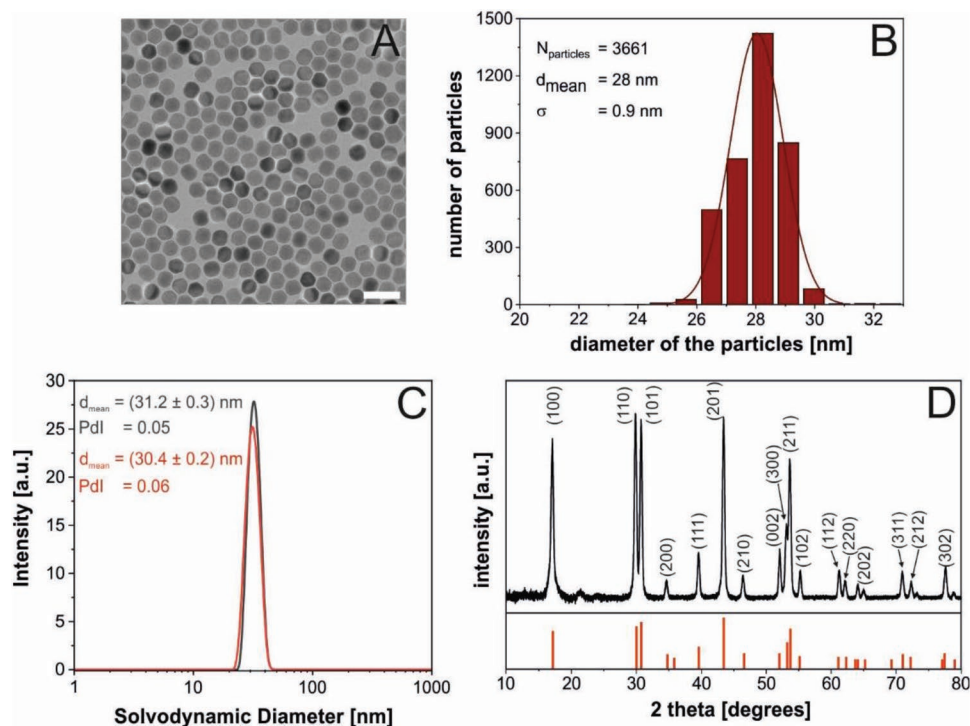The ORCID identification number(s) for the author(s) of this article can be found under https://doi.org/10.1002/ppsc.201900235.

**ADVANCED
SCIENCE NEWS**
www.advancedsciencenews.com

Particle
& Particle Systems Characterization
www.particle-journal.com

Figure 1. A) Transmission electron micrograph (scale bar: 60 nm) and B) corresponding size distribution of oleate-capped NaYF$_4$(20%Yb, 2%Er). C) Intensity-weighted particle-size distribution obtained by dynamic light scattering of a particle dispersion in cyclohexane (≈5 mg mL^{-1}, $n = 3$) of UCNPs shortly after the synthesis (red) and after a storage of ≈4 years (gray). D) X-ray diffraction patterns of UCNPs. The pattern in red refers to the standard pattern (ICDD PDF #16-0334) of hexagonal phase NaYF$_4$.

introducing functionalities such as receptors for targeting or labels for imaging. In this study, the colloidal and chemical stability of NaYF$_4$(Yb,Er) nanoparticles modified by five different surface coatings via a two-step ligand exchange assisted by NOBF$_4$ has been investigated in detail. As this method is not only one of the most versatile ones,[26] but also fast and easy to handle, we have focused on this strategy. Regarding the colloidal stability, the relevant forces within a nanoscopic system must be taken into account. Particles without any surface capping tend to minimize their surface energy by aggregation so that further efforts are inalienable to obtain stable nanoparticles.[27]

The five different surface ligands attached to UCNPs of identical size consist of three polymers (poly(acrylic acid) (PAA), polyallylamine (PAH), and polyethylene glycol (PEG)) and two small ligands (citrate (CIT) and N,N bis(phosphonomethyl)glycine (PG)). This set of particles was used to investigate the concentration dependent colloidal and chemical stability in water over time. Detailed information is presented on different coordination groups stabilizing the particles and how the disintegration of the particles is influenced by ions present in the solution.

2. Results and Discussion

2.1. Synthesis and Design of Hydrophilic Upconversion Nanoparticles

Predominately green emitting UCNPs based on the most common host material NaYF$_4$ with a doping ratio of 20% Yb^{3+}

and 2% Er^{3+} have been synthesized on large-scale by a bottom-up approach.[28] The oleate coated particles of pure hexagonal crystal phase show a diameter of 28 ± 0.9 nm with a narrow size distribution (**Figure 1** A,B,D) and a phonon energy of 300 cm^{-1} determined via Raman spectroscopy (Figure S1, Supporting Information). Dynamic light scattering (DLS) measurements of UCNP dispersion (≈5 mg mL^{-1}) revealed the outstanding long-term colloidal stability of the nanoparticles for at least 4 years in organic solvents (Figure 1C).

The doping ratio of the lanthanide ions in the particles matches the ratio of the respective lanthanide chlorides used in the synthesis as confirmed via mass spectrometry combined with inductively coupled plasma (ICP-MS) measurements (Table S1, Supporting Information). These UCNPs co-doped with Yb^{3+} and Er^{3+} show emissions at 522 nm ($^2H_{11/2} \rightarrow {}^4I_{15/2}$, green), 540 nm ($^4S_{3/2} \rightarrow {}^4I_{15/2}$, green), and 650 nm ($^4F_{9/2} \rightarrow {}^4I_{15/2}$; red) (**Figure 2**) upon excitation with a low-power 980 nm laser module. The absorption cross-section of the Yb^{3+}-ions within the nanocrystal was estimated to be ≈(2.5 ± 0.1) × 10^{-20} cm^2 (Table S2, Supporting Information), which corresponds to the value reported in the literature.[29] For the green emission, a decay time of (156 ± 1) µs and for the red emission one of (226 ± 3) µs was measured with a home-built lifetime-setup (Figure S2, Supporting Information).

Five different surface-modifications (UCNP@CIT, UCNP@PAA, UCNP@PEG, UCNP@PAH, and UCNP@PG) have been chosen to study the colloidal and luminescence properties of these particles in water. All surface modifications have been prepared from the same batch of oleate capped
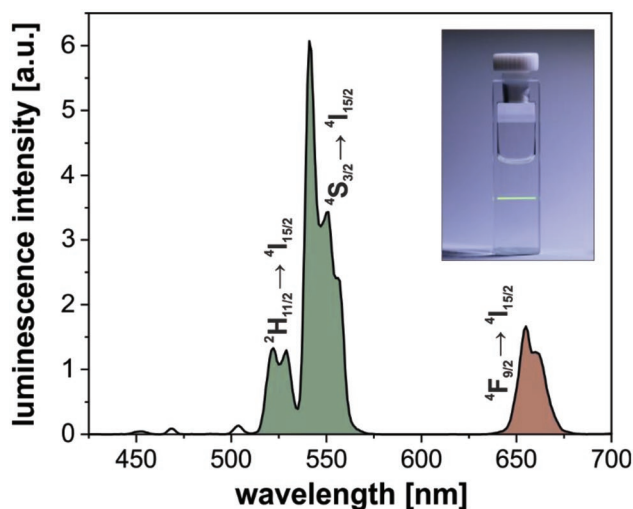
Figure 2. Luminescence spectrum of NaYF$_4$(Yb,Er) dispersed in cyclohexane (13 mg mL^{-1}). A 980 nm CW laser module (200 mW, 15 W cm^{-2}) was used as excitation source. In the insert one can see a digital photograph of UCNPs coated with oleic acid under NIR excitation.

particles via a ligand exchange process assisted by NOBF$_4$ (**Figure 3**).[30,31]

In the first step, the hydrophobic oleate-capped UCNPs (UCNP@OA) in cyclohexane are mixed with an equivalent volume of DMF leading to a two-phase system. After the addition of NOBF$_4$ a slightly acidic environment is created, as the NO$^+$-ions react with water residues in the DMF and forms nitrous acid and H$^+$ as reported in the literature (Equation (1))[31]

$$NO^+ + H_2O \rightleftarrows HNO_2 + H^+ \qquad (1)$$

It is desired to strip off the oleate completely. Therefore, an excess of protons is needed. The coverage of oleate on the surface of UCNPs is 60%, determined by thermal gravimetric analysis (TGA) (Figures S3 and S4, Supporting Information). Under the assumption that all H$^+$ required for this process, come from the reaction of residual water in DMF ($\approx$0.2% determined via Karl Fischer titration, Figure S5, Supporting Information) with NO$^+$, the minimal required amount of water is depending on the size of the nanoparticles, e.g., for the 28 nm sized UCNPs $\approx$7300 water molecules per particle are needed (Figures S4 and S6, Supporting Information).
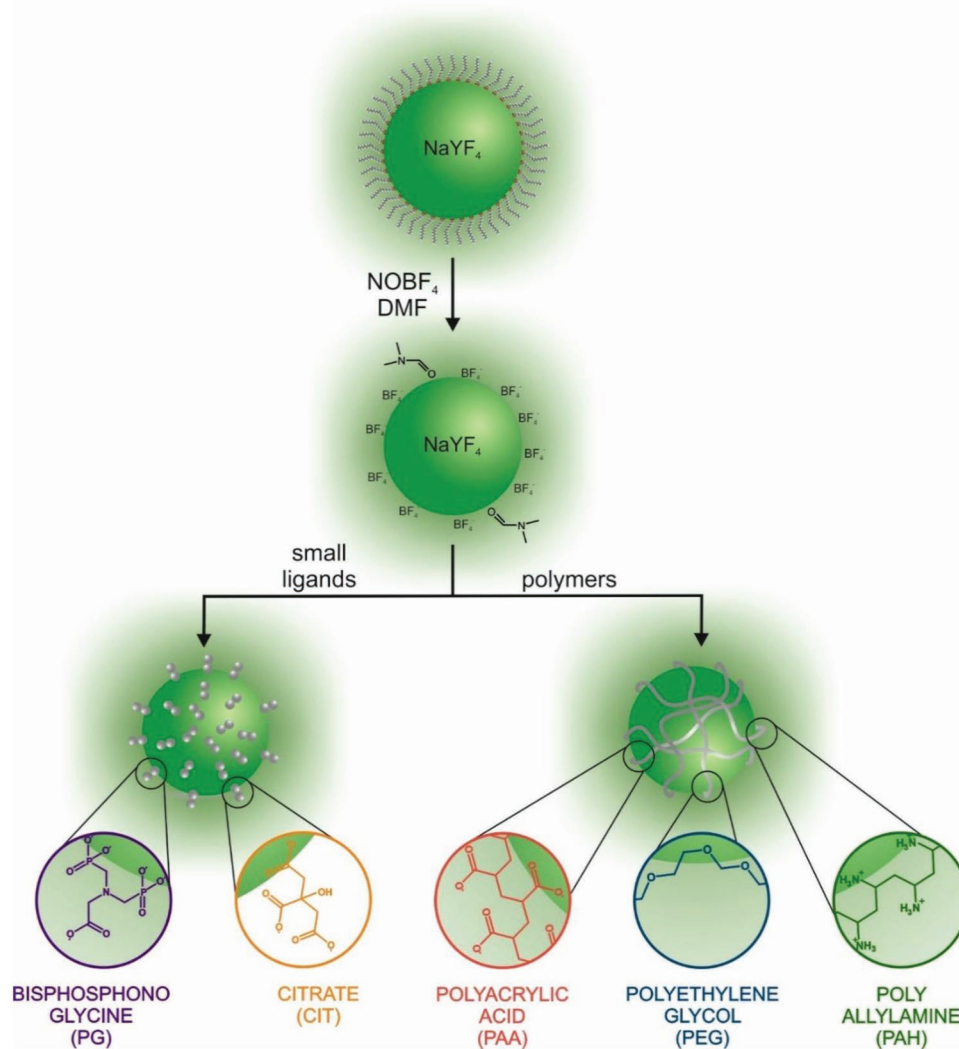
In the course of the reaction, the oleic acid gets removed from the surface of the nanoparticles remaining in the cyclohexane phase. The UCNPs are transferred to the DMF phase, where they are stabilized by BF$_4^-$ (UCNP@BF$_4$). As shown by Fourier-transform infrared (FTIR)-spectroscopy, the typical vibrations of oleic acid can be found only in the cyclohexane phase (Figure S7, Supporting Information). After $\approx$15 min the phase transfer is complete, and no upconversion luminescence can be excited any longer in the cyclohexane phase. The total yield and the composition of the BF$_4^-$ stabilized nanoparticles has been determined via ICP-MS to be $\approx$95% (according to TGA, $\approx$8250 BF$_4^-$ molecules coordinate to the surface of one nanoparticle). Figure S8 (Supporting Information) shows the particle-size distribution of BF$_4^-$-stabilized UCNPs in DMF in

comparison to UCNPs with oleate capping in cyclohexane, indicating colloidal stability of the particles in DMF after the ligand removal due to weakly coordinating BF$_4^-$ ions.[32]

To complete the phase transfer, BF$_4^-$ stabilized UCNPs dispersed in DMF are mixed with an aqueous solution, containing the desired hydrophilic surface ligand. For this study small molecules (like PG and CIT) and polymers (PAH, PAA, and PEG) have been investigated in detail. It has to be mentioned that also the composition of the UCNP has to be considered when thinking on the coordination of ligands to the particle surface, as different lanthanide ions prefer different coordination numbers.

Within a nanocrystal, consisting of NaYF$_4$, the Y^{3+} ions are coordinated by nine neighboring ions as shown by molecular dynamics simulations.[33] At the surface of bare particles, this number is unsaturated due to the missing of coordination partners and it is possible for ligands to attach via coordination toward the Y^{3+} ions. In principle, a large number of free electron pairs provided by the surface ligand could lead to the maximum coordination number. In contrast to this, sixfold coordination is more likely for Yb^{3+} ions.[34] Thereby, changes in the surface coverage as well as in the binding stability for different host materials (e.g., NaYF$_4$ or NaYbF$_4$) are expected. Additionally, the shape of the nanoparticles is essential. As shown by the group of Jin[35] phosphate headgroups are capable to coordinate with up to three oxygen atoms toward the Y^{3+}. However, the binding energies of the ligands at rod-like structures (hexagonal prism) are changing with the crystal plane, allowing anisotropic surface modifications.

The oleate can also be stripped off by an alternative method, where the particle dispersion is treated by an acid, most likely HCl.[20,36–38] Thereby the hydrophobic oleate capped UCNPs need to be dispersed in an acidic aqueous system for 2 h (Figure S9, Supporting Information). Regarding the pK_a of the ligand, which needs to be replaced from the particle surface, the reaction protocol has to be adjusted in terms of reaction time and pH. For the oleate capped particles used in this study, pH 3 and 2 h reaction time are sufficient. This method is somehow trickier than the ligand exchange via BF$_4^-$, as the mixing of the hydrophobic particles with the acidic aqueous phase can come with difficulties, and also due to the tendency of bare particles to minimize their surface energy by forming agglomerates (Figures S10 and S11, Supporting Information). Therefore, it is not surprising that the yield of this method is only in the range of 30–35%, according to the ICP-MS measurements. In contrast, the ligand exchange with the BF$_4^-$ mediated method yields up to 95%. When comparing both methods for an identical particle system, it was found that the surface coverage achieved by the acid mediated ligand exchange is slightly higher compared to the BF$_4^-$ mediated ligand exchange (Figure S3, Supporting Information). In case of PG as new surface ligand, $\approx$1600 molecules get attached to the surface of the nanoparticles. For the two-step ligand exchange, only $\approx$1200 molecules have been bound. The reason might be, especially for this surface ligand that the pH was more acidic and therefore not all groups of this ligand have been deprotonated. By this, the electrostatic repulsion between two neighboring surface ligands might be lower, which minimizes the distance and therefore leads to a

ADVANCED
SCIENCE NEWS
www.advancedsciencenews.com

Particle
& Particle Systems Characterization
www.particle-journal.com

Figure 3. Scheme of the two-step ligand exchange for the surface modification of upconversion nanoparticles. In the first step the oleate is removed via the addition of $NOBF_4$. The bare UCNPs are stabilized via BF_4^--ions. In the next step the particles are modified with the desired ligand (here PG, CIT, PAA, PEG, and PAH).

higher surface coverage. By directly comparing both methods, the ligand exchange with $NOBF_4$ shows several advantages: Besides the short reaction time and easy purification protocol, the particles are electrostatically stabilized throughout the whole process, which reduces the aggregation during the ligand exchange process and increases the yield of the modified UCNPs.

2.2. Differences of the Surface Coverage by Using Small Ligands and Polymers

Phosphate groups show a very high binding affinity followed by carboxylic groups, when looking at the binding ability of the functional group of the ligand toward the surface of the nanoparticles.[17] Nevertheless, also amine groups[30] and ether groups[39] are capable to coordinate to the lanthanide ions to obtain water dispersible nanoparticles. Consequently, all these

kinds have been investigated regarding colloidal as well as chemical stability in aqueous solutions.

PG, with two phosphate groups, is expected to coordinate best to the UCNPs but a surface coverage of only ≈20% (Figure S3, Supporting Information) was found (≈1200 PG ligands per UCNP (size 28 nm)). Such low coverage can be explained by electrostatic effects. At neutral pH, PG is four times negatively charged, which leads to a strong electrostatic repulsion at the surface of one nanoparticle (Figure S12, Supporting Information). Therefore, it is quite obvious that those surfaces cannot be densely covered, a distance between two neighboring PGs can be calculated to be 1.6 nm. Completely different is the situation when a capping agent like poly(acrylic acid) is used. The polymer PAA ($M_W \approx 2.1$ kDa) used here consists in average of 30 monomers with each of them providing a carboxylic group, which can bind to the surface of the nanoparticles. From TGA characteristics one can calculate from the loss of the total mass that ≈520 polymers have been attached to the

ADVANCED
SCIENCE NEWS
www.advancedsciencenews.com

Particle
& Particle Systems Characterization
www.particle-journal.com

surface of one nanoparticle. The analysis of the particle size by DLS (as well as the particle distance on the transmission electron microscopy (TEM) grid) indicates that the polymer forms only a thin layer. Similar findings have been reported for iron oxide particles covered by PAA.[40] A very simplified assumption that all monomers can coordinate to the particle surface reveals a coverage of 120%. This demonstrates that a large fraction of the polymers does not bind with all carboxylates to the surface. The other extreme would be that the polymers are linked only by one single carboxylate to the surface (surface coverage of 4%) with a distance of 2.4 nm to the next neighbor. This is also quite unexpected, and the reality should be somewhere in between.

Especially changes in pH might lead to more or fewer charges at the surface of the particles and prevent a dense surface coating due to electrostatic repulsion. In contrast to PG, PAA molecules are bearing more than one surface charge. In this case, an electrostatic repulsion of the charges is limited due to the polymeric nature of the capping agent. Complementary to the work of Joshi and co-workers,[41] the PAA molecules can be seen as crosslinked monomers bearing only one charge. A first glance at the Coulomb-potential shows that systems with a small charge show less repulsion leading to a lower distance between the surface ligands. For an even more detailed description of the electrostatic repulsion of the PAA polymers, it would be interesting to calculate the Coulomb-potential based on the charge density of the polymer (e.g., via molecular dynamics simulations).

2.3. Colloidal Stability of Hydrophilic Upconversion Nanoparticles

By comparison of the ligand exchange for small molecules and polymers, one can clearly see the advantage of the larger surface capping. Besides the higher surface coverage of the particles also a huge number of functional groups can contribute to the colloidal stability of these systems and create a dense surface coating. In the case of polymers with strongly coordinating groups like the carboxyl in PAA, the smaller hydrodynamic diameter indicates that the polymer gets tightly wrapped around the particle. For polymers with ether groups (like PEG) or with amine functionalization (PAH), the coordination to the Y^{3+} is slightly weaker. For instance, at pH 7, a large fraction of the amine groups is protonated so that only a few binding sites would be available, leading to a weaker attachment of the polymer chain toward the surface of the particles. An increased hydrodynamic diameter is the consequence of this. For small molecules like PG, steric reasons prevent the coordination via all possible groups and therefore a larger hydrodynamic diameter may be found. Despite the low surface loading of the PG molecules, the PdI of those UCNPs is in the same range as for UCNPs with polymer coating or with a CIT capping. Also, from TEM studies, no agglomerates are found, and the clear dispersion of the UCNPs prove the colloidal stability of the nanoparticles (**Figure 4** and Figure S13A, Supporting Information).

As seen from Table S3 (Supporting Information), the surface ligands not only differ from their binding groups and size (small molecules vs polymers), but also from their charge (Figure S3.13B, Supporting Information). At pH 7, PG bears

four negative charges, whereas CIT is three times deprotonated. The difference of the charge of the surface ligands can also be seen in the ζ-potential. UCNP@PG have a slightly more negative ζ-potential than UCNP@CIT. In the case of polymers like PAA, which cannot distribute their charges by electrostatic repulsion, because of their linkage by chemical bonds, a higher surface coverage compared to the small capping molecules is expected. This is also indicated by a higher ζ-potential (Figure 4). In the case of the PAH—which has positively charged amine groups—a similar interaction of the polymer toward the nanoparticle as described for the PAA molecules is present. Consequently, the average surface charge is quite similar, as seen for the PAA.

All hydrophilic UCNPs can be excited with a 980 nm CW laser module and the typical upconversion emission spectrum of Yb^{3+}/Er^{3+} co-doped nanoparticles can be obtained (Figure S14, Supporting Information). In contrast to the oleic acid capped UCNPs in cyclohexane, the ratio between the green and the red emission band is decreased due to the presence of water quenching. Whereas it is ≈3.7:1 for UCNP@OA, I_{green}/I_{red} is ≈2.8:1 for all types of the here studied hydrophilic UCNPs. This indicates that the shielding against water access to the surface of the particles is very similar for all types of surface modification and still many lanthanide ions seem not to be completely coordinated by a surface ligand. At those ions, water might act as ligand and consequently quench the upconversion luminescence.

By using the particles for bioanalytical applications often not only the stability of the system in water but also under the influence of highly ionic strength needs to be considered as reported in literature.[42,43] Therefore, the colloidal stability of the particles was investigated in different NaCl solutions ranging from 0 to 2.5 M. For UCNP@CIT and UCNPs@PG the increasing ionic strength leads to the formation of strong aggregations as seen in Figure S15 (Supporting Information). For particles capped with a polymer (UCNPs@PAA, UCNP@PAH, and UCNP@PEG) remarkably colloidal stability up to 2.5 M was observed. The reason for this different behavior can be explained by the different nature of the surface ligands. Whereas the small molecules only lead to electrostatic stabilization, the polymer ligands provide additional steric hindrance.

2.4. Long-Term Stability of Aqueous Dispersions of Upconversion Nanoparticles

UCNPs with a $NaYF_4$ host lattice have been associated for a long time with excellent chemical stability[7,44–46] and show a very low solubility product of 1.6×10^{-26} M^6.[47] Nevertheless, a small amount of the particles gets dissolved[38,47–49] in water according to the equilibrium reported by the group of Mely[47] and displayed in the following equation:

$$NaYF_4 \rightleftharpoons Na^+ + Y^{3+} + 4F^- \tag{2}$$

In a saturated solution the concentration of the free ions ($[Na^+]$, $[Y^{3+}] = 20 \times 10^{-6}$ M, $[F^-] = 80 \times 10^{-6}$ M, refer to S6.15 in the Supporting Information) is very low. For a typical stock solution consisting of $NaYF_4(20\%Yb, 2\%Er)$ nanoparticles
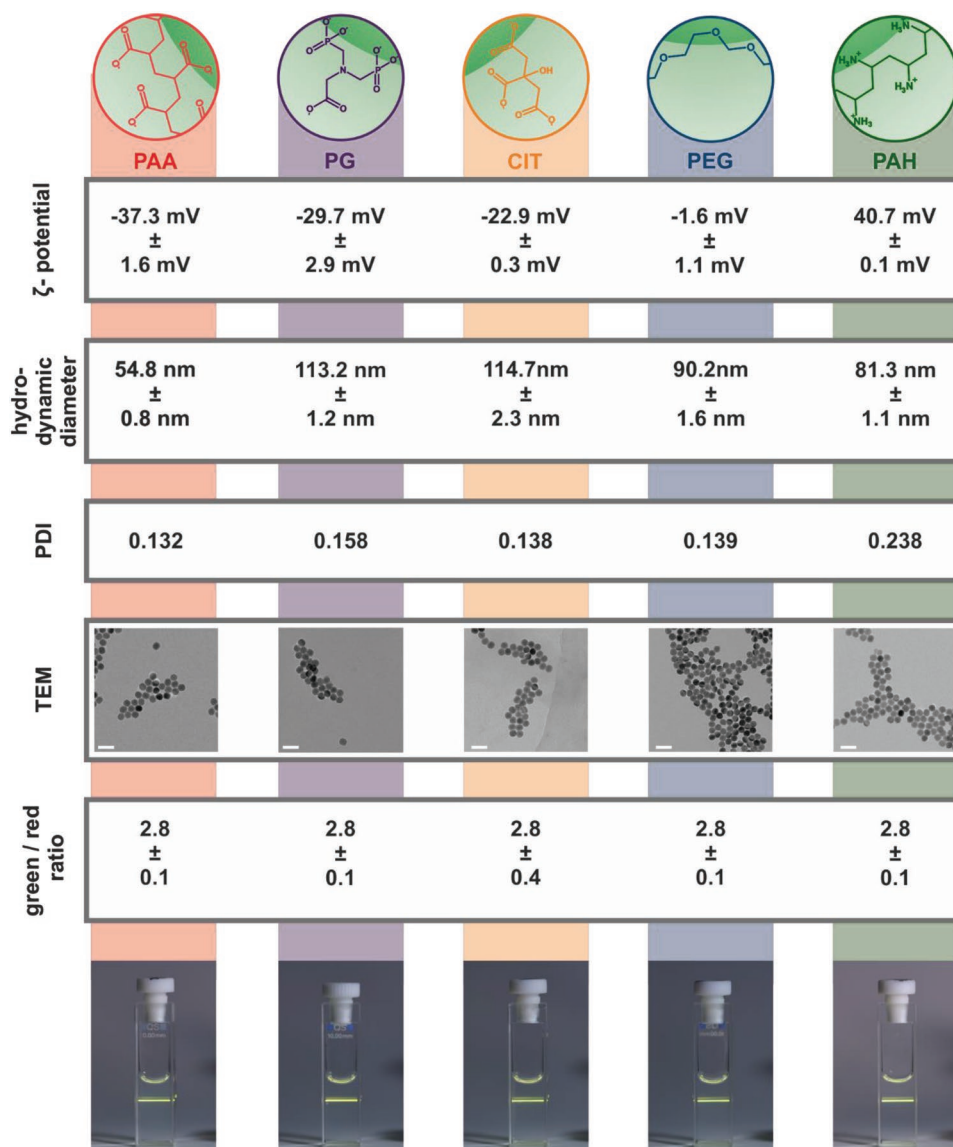
Figure 4. Overview of the ζ-potential measurements, intensity weighted dynamic light scattering measurements, and TEM measurements for all particle systems. At the bottom digital photographs of each particle system under 980 nm laser excitation (200 mW, CW, 1.6 mg mL^{-1}), with corresponding ratio of the emission intensity at 540 nm and 650 nm, are shown. The clear dispersions are an indication for colloidal stability.

(28 nm, 5 mg mL^{-1}), the amount of fluoride within the nanoparticle is around 900 times higher. Only a neglectable part of about 0.1% of the total F$^-$ ions will get dissolved in steady state conditions. Highly diluted systems as often used in biological applications, with a mass concentration of 100 µg mL^{-1} of UCNPs and lower become critical. Here, ≈5% of the ions get dissolved until the solution reaches its equilibrium.

As seen from the TEM images (Figures S16 and S17, Supporting Information) at 100 µg mL^{-1} dilution, the morphology of the UCNP@PAH is almost not affected compared to UCNP@OA or UCNP@BF$_4^-$. This has also been confirmed by the luminescent signal at 540 nm as well as by the hydrodynamic diameter, which both remain quite constant (Figure S18, Supporting Information). Further reduction of the particle concentration leads to a higher dissolution rate (Figure S19,

Supporting Information). This has a tremendous influence on the storage and usage of highly diluted dispersions of upconversion nanoparticles. For instance, in UCNPs dispersions with 10 µg mL^{-1} ≈50% of the particles will get dissolved in a short period of time (Figure S20, Supporting Information). Already 2.5 h after dilution the luminescence signal and size of the nanoparticles was strongly reduced. Mainly for in vivo/in vitro applications, the mass concentration is essential. As shown in Table S4 (Supporting Information), cytotoxicity studies are typically covering this range of concentrations. Due to the dissolution of the nanoparticles, one has to consider the potential toxic influence of the released F$^-$ ions. In contrast, the amount of UCNPs for applications in vivo is often higher (the final concentration in, e.g., a mouse (≈25–35 mg, 1.5 mL blood volume) is ranging between 150 and 3000 µg mL^{-1}) so that in steady state
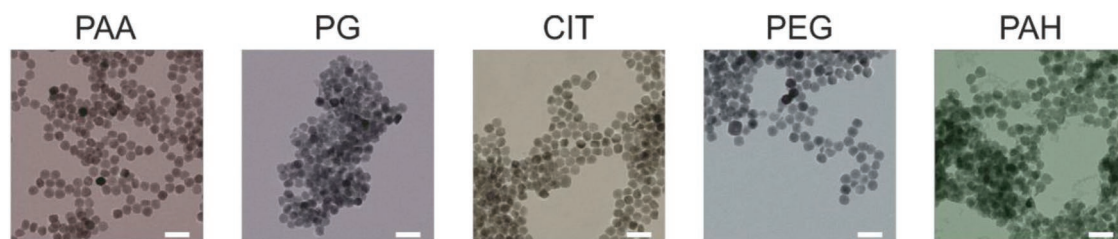
Figure 5. TEM images of UCNPs (100 µg mL^{-1}) with different surface capping (red = PAA, purple = PG, orange = CIT, blue = PEG, and green = PAH) after dialysis for 300 min. In the case of a capping with small molecules, aggregation and strong dissolution can be observed. Dissolution effects can also be seen for UCNPs modified with PAH and PEG. UCNP@PAA are more prone to those effects.

after dissolution of the particles the luminescent properties will only be minimally affected.

Analogous to the different surface coverage also the chemical stability and dissolution behavior of the UCNPs at high dilutions is affected by the presence of small molecules or polymers (**Figure 5**). A closer look at the negatively charged nanoparticles including UCNPs with CIT, PAA, and PG showed no good protection against dissolution. Particles with these surface ligands are characterized by a constant drop in the upconversion luminescence when dialyzed for 24 h. In each case, the luminescent intensity already at a high mass concentration of 5000 µg mL^{-1} showed a drastic reduction of the luminescence at 650 nm (Figure S21, Supporting Information) and at 540 nm (Figure S22, Supporting Information). Both UCNP@CIT and UCNP@PAA still retained ≈30% of the initial luminescence intensity, whereas for UCNP@PG only ≈15% of the original signal can be measured. An explanation can be found by analyzing the particles by DLS and TEM (Figure S22, S23–CIT, S24–PG, and S25–PAA, Supporting Information), which indicates an ongoing aggregation of the particles especially for the PG modified UCNPs. Particles with PAA capping are much longer resistant to those aggregation effects.

The increase of the PdI with time is another hint for the instability of these systems (Figure S26, Supporting Information). On the first glance, an inconsistency of the DLS data with obtained those from luminescence measurements and the electron microscopy might be suspected, but from the complete data set of complementary methods, one can suggest that the aggregation with following precipitation was the reason for the loss of luminescence. Therefore, it is not easy to make an assumption from data obtained only by one single technique.

For diluted dispersion of UCNPs (Figures S27 and S28, Supporting Information), the colloidal as well as the chemical stability is affected as expected. The low surface coverage of the small molecules does not sufficiently protect the particle surface against dissolution. Already after 450 min of dialysis for concentrations of 1000 µg mL^{-1}, a slight change of the morphology of the nanoparticles and a decrease in the upconversion luminescence intensity was observed (Figure S27, Supporting Information). By using a dispersion with 500 µg mL^{-1} the luminescent signal almost vanished for UCNP@CIT and UCNP@PG after 24 h of dialysis (Figure S28, Supporting Information). For even lower particle concentrations (100 µg mL^{-1}), the disintegration (strongly) affects the morphology and size of all negatively charged nanoparticles as seen in the TEM images

(Figure 5). Accompanied by this, a strong loss of the upconversion efficiency as well as an increase in the hydrodynamic diameter due to the agglomeration of the fragmented particles is found.
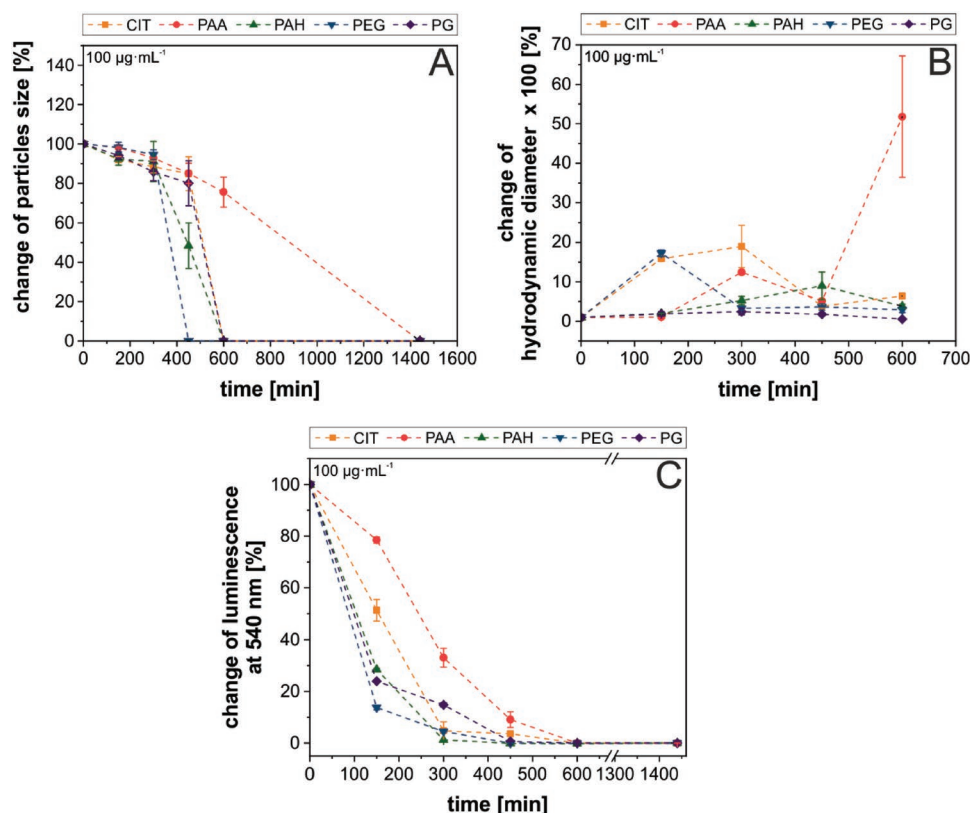
The dissolution of particles at the smallest concentration reveals again a different trend between the three negative surfaces. For particles modified with small ligands like PG already after 150 min ≈70% of the luminescence signal has vanished. For UCNPs with CIT capping a decrease of the luminescence to 30% has been observed after ≈200 min. In contrast to this, PAA modified particles were the most stable ones. After 300 min, the relative change of the luminescence signal has decreased to 30% (**Figure 6**).

For UCNPs with PEG groups at the first glance a much more stable system seems to be present. As seen in Figure S29 (Supporting Information) at the highest concentration, the particles are nearly unaffected in their stability. However due to the weaker binding of the ether groups toward the nanoparticles, at a mass concentration of 1000 µg mL^{-1} (after 450 min) also a slight deformation of the nanoparticles can be observed and after 24 h the luminescent signal decreases to 70% (Figure S27, Supporting Information). Further dilution to 100 µg mL^{-1} leads to a similar course as for the other UCNPs (Figures 5 and 6). After ≈150 min, around 70% of the initial luminescence at 540 nm has vanished.

Remarkably colloidal and chemical stability was found for UCNPs functionalized by positively charged PAH (Figure S30, Supporting Information). At a high mass concentration of 5000 µg mL^{-1} the upconversion luminescence was almost not affected at all during a dialysis period of 24 h. However, also here for the smaller amount (1000 µg mL^{-1}) a slight change of the morphology of the nanoparticles and an influence on the emission intensity has been observed. Further reduction of the mass concentration to 100 µg mL^{-1} leads to a loss ≈70% of the initial luminescence signal (Figure 6) after only 150 min of dialysis.

2.5. Stabilizing Strategies for Highly Diluted Aqueous Upconversion Nanoparticle Dispersions

Due to the poor stabilization of the UCNPs via hydrophilic surface ligands directly attached to the particle surface one of the simplest possibilities to prevent the particle dissolution is given by the addition of respective ions to the dispersion media. For applications without toxicity issues, this might not be a

**ADVANCED
SCIENCE NEWS**
www.advancedsciencenews.com

Particle
& Particle Systems Characterization
www.particle-journal.com

Figure 6. Analysis of the colloidal and chemical stability of UCNPs with different surface capping (PAA, PAH, PEG, PG, and CIT) and with a mass concentration of 100 μg mL^{-1}. A) Change of particle size analyzed via TEM. B) Change of hydrodynamic diameter determined via intensity-weighted dynamic light scattering measurement. C) Change of luminescent signal at 540 nm for different times and surface capping. The particles were excited with a 980 nm laser module (200 mW, CW).

problem at all. For single particle imaging as shown by the group of Mely[47] UCNPs based on NaYF$_4$ host materials stay stable when 1 mmol L^{-1} fluoride was added to the solution. In order to study the presence of different ions for the stability of PAH and CIT modified UCNPs dialysis not only against water but also against 1×10^{-3} M KF solution, 1×10^{-3} M NaNO$_3$, a solution with 100 μg mL^{-1} of the ligand (e.g., PAH or Na$_3$CIT), 1×10^{-3} M Y(NO$_3$)$_3$, and 1×10^{-3} M of KF and Y(NO$_3$)$_3$ has been performed. Additional F$^-$ ions can entirely hinder the dissolution of highly diluted UCNPs due to the exceedance of the saturation concentration of the free F$^-$. As seen in the TEM images of UCNP@PAH (Figure S31, Supporting Information) and UCNP@CIT (Figure S32, Supporting Information), the morphology of the particles at high dilution (100 μg mL^{-1}) remains constant for 24 h.

In the case of Y^{3+} the equilibrium could be reached by a mechanism reported by the group of Liu.[50] They describe a change in the nanoparticle composition by cation exchange. Theoretically, surface-bound Yb^{3+} and Er^{3+} ions could be exchanged by Y^{3+}, ideally leading to an "inert shell" preventing surface quenching of the upconversion luminescence. For the 28 nm sized particles, after dialysis against a pure Y(NO$_3$)$_3$ solution, this could not be found. The different lanthanide ions have individual solubility constants, so that only the pathway with Y^{3+} disintegration is hindered, but the dissolution mechanism based on Yb^{3+} and Er^{3+} is still possible and leads to a drastic change of the morphology of the particles, as seen

from the TEM images (Figures S31, S32, and S33, Supporting Information).

By applying a mixture of KF and Y(NO$_3$)$_3$ the dissolution can be prevented. For a short dialysis time (≈up to 450 min) indeed an increase of the upconversion signal at 540 nm can be observed for UCNP@PAH (Figure S33, Supporting Information). However, a closer look at the TEM showed no monodisperse UCNPs any longer, as spark-like structures have grown around the particles. It is assumed that YF$_3$ is deposited on the UCNPs. In contrast to the UCNP@PAH, negatively charged UCNP@CIT suffer from fast crosslinking and aggregation. As shown by the group of Xu, the carboxylic groups of, e.g., the poly(acrylic acid) are capable to complex lanthanide ions.[51] This effect has to be considered as the negatively charged UCNPs can interact with the Y^{3+} ions and lead to a crosslinking of the particles as schematically shown in Figure S34 (Supporting Information). Thereby especially systems with a low number of surface ligands and a low number of functional groups—like is the case for CIT and PG capped UCNPs—already minimal amounts of Y^{3+} would lead to strong crosslinking. For UCNP@PAA, were crosslinking is also a problem, the high number of functional groups prevents a complete aggregation of the colloidal system, when only a small amount of the Y^{3+} is present. To study the phenomenon of Ln^{3+} induced crosslinking in a dispersion of UCNP@PAA (1000 μg mL^{-1}) small amounts of Y^{3+} were added and their luminescence and colloidal properties were monitored

**ADVANCED
SCIENCE NEWS**
www.advancedsciencenews.com

Particle
& Particle Systems Characterization
www.particle-journal.com

over time. As seen in Figure S35 (Supporting Information) with the addition of more and more Y^{3+}, an increase of the hydrodynamic diameter was measured. With increasing concentration of Y^{3+}, the colloidal stability of the nanoparticles gets affected very strongly, leading to large aggregates and a decrease of the luminescence at 540 nm. In the presence of 200×10^{-6} M EDTA this effect can be shifted to higher concentrations of Y^{3+}, as EDTA complexes the Y^{3+}.

Due to the potential toxic effect of added fluoride ions and the limitation of this in the aspect of bioanalytical applications, it was also studied if the addition of the ligand itself or the addition of Na^+ would have a positive effect. However, for the dissolution of the nanoparticles not only the pathway in Equation (2) but also a second one, described by the group of Mely,[47] would be possible

$$YF_3 \rightleftharpoons Y^{3+} + 3F^- \qquad (3)$$

Therefore, the addition of Na^+ only hinders the pathway according to Equation (2), as it exceeds the saturation concentration of Na^+ ions associated with the UCNPs. The one following Equation (3) is still possible. Due to the limitations to this route, the dissolution process is slowed down as seen from the TEM images (Figures S31, S32, and S33, Supporting Information). The same phenomenon can be observed when using Na_3CIT as an additive for CIT capped UCNPs. The addition of a solution with only the ligand (PAH for PAH capped UCNPs) does not hinder the disintegration of the nanoparticles. Additionally, to the change of the morphology also the influence of the dissolution on the crystal structure of the nanoparticle was analyzed (Figure S36, Supporting Information). In each case, whether the particles are stabilized via KF or get partly dissolved, no change of the lattice constant can be observed. This indicates that the KF prevents the leakage of the F^- ions. In the presence of both KF and $Y(NO_3)_3$ a "shell" is grown around the particles and for UCNP@PAH no crosslinking of the YF_3 shell occurs. It grows uniformly in one direction and also the lattice constant is still 0.5 nm.

3. Conclusion

In this study five different surface capping ligands—poly(acrylic acid), polyallylamine, citrate, phosphonoglycine, and polyethylene glycol—were examined in terms of their shielding ability for long-term colloidal stability of $NaYF_4(Yb,Er)$ upconversion nanoparticles in aqueous dispersions of low concentration.

The surface modification was performed by NOBF4 assisted two-step ligand exchange, resulting in colloidally stable aqueous dispersions, when stored at high concentrations, as demonstrated by a low polydispersity index. For colloidal stability, both the attractive van der Waals interaction of two particles ($E_{v.d.W.}$) and the repulsive forces due to the surface capping are essential. The luminescence data of UCNP@PAA, UCNP@PAH, and UCNP@PEG do not indicate better shielding, and the hydrodynamic diameter of those modifications was in the same range as for surface coatings assembled by small molecules. It is assumed that the high colloidal stability at neutral pH is achieved by electrostatic repulsion of the nanoparticles due to charged molecules attached to the nanoparticle surface.

Consequently, for the design of a hydrophilic surface, providing colloidal stability for the whole physiologically relevant pH range, the ligands should consist of molecules providing both, steric hindrance as well as electrostatic repulsion.

Under nonsteady state conditions like it is the case in flow systems for online monitoring or in high dilutions as for single particle imaging, the ligand-exchange method does not end up with a surface modification providing a tight coating to prevent particle disintegration with time. Due to the dominant electrostatic stabilization, almost identical low surface coverage rates have been found without any significant influence of the type of ligand. As a consequence, surfaces with a strong negative ζ-potential tend to aggregate in highly dilutions or in flow conditions already after a short period of time despite their theoretical high colloidal stability. A closer examination revealed that released Ln^{3+} might crosslink with the negative charged carboxylic groups and limit the colloidal stability of those systems. In contrast, UCNPs with PAH and PEG capping did not show this Ln^{3+} induced colloidal instability. However, by strong dilution of all examined particle systems, a strong loss of the luminescence due to the dissolution of the nanoparticles has been observed. The easiest way to prevent disintegration is given by the presence of fluoride ions in solution. Here one has to keep in mind that changes in the ionic strength of the dispersion media will also have an impact on the electrostatic stabilization. Therefore, this parameter will also be investigated, together with surface ligands that have been reported for colloidal stability via steric repulsion,[52,53] in the near future.

4. Experimental Section

Chemicals: Oleic acid and 1-octadecene (both technical grade, 90%) were purchased from Alfa Aesar (www.alfa.com). Lanthanide chloride hexahydrates ($YbCl_3 \cdot 6H_2O$, $YCl_3 \cdot 6H_2O$, and $ErCl_3 \cdot 6H_2O$ each >99.99%) were obtained from Sigma Aldrich and Treibacher Industrie AG. Ammonium fluoride, sodium hydroxide (both analytical grade), nitrosyl tetrafluoroborate (95%), *N,N* bis(phosphonomethyl)glycine (PG, 98%), sodium fluoride (KF), ytterbium nitrate ($Y(NO_3)_3$), poly(acrylic acid) sodium salt (PAA, $M_w \approx 2100$), trisodium citrate (CIT), polyallylamine hydrochloride (PAH, $M_w \approx 15\,000$), polyethylene glycol ($M_w \approx 12\,000$) and ethylenediaminetetraacetic acid (EDTA) were obtained from Sigma Aldrich. The water standard (Aquastar, 5 mg mL^{-1}) and the CombiCoulomat fritless Karl Fischer reagent were purchased from Merck. All other chemicals were of analytical grade. All chemicals were used as received without further purification. Double distilled (dd) water was used for the preparation of all aqueous solutions.

Characterization and Measurement Methods: Transmission electron microscopy was carried out with a 120 kV Phillips CM12 microscope. For sample preparation, a particle dispersion ($\approx$1.5 mg mL^{-1} in cyclohexane or dd water) was dropped on a copper grid (coated with carbon, 400 mesh). The obtained micrographs were analyzed with the software ImageJ. Dynamic light scattering and ζ-potential measurements were carried out on a Malvern Zetasizer Nano ZS at 20 °C. For the determination of the particle concentration and the doping ratios of the rare-earth ions within the UCNPs, mass spectrometry combined with inductively coupled plasma (ELAN 9000 from Perkin Elmer) was used. For calibration, a multielement standard solution from Perkin Elmer (10000 ppb with various dilutions ranging between 200 and 1 ppb in 5% HNO_3) was utilized. A rhodium standard solution (10 000 ppb) in 5% HNO_3 dealt as internal standard. Upconversion samples were prepared by an acidic decomposition of the nanoparticles ($\approx$0.3 mg) in 417 µL H_2SO_4 (96% w/v) assisted by ultrasonication. Afterward, the solution

was diluted by the addition of 7.083 mL water and 7.5 mL 1 M HNO$_3$. For the ICP-MS measurement, the particles (1 mL) were diluted additionally with 49 mL 5% HNO$_3$ and 10 µL of the rhodium standard was added.

For Raman measurements, a DXR Raman microscope from ThermoFischer equipped with a 100 × magnification Mplan N objective, a 532 nm laser excitation (0.5 mW) and a 50 µm slit was used. X-ray diffraction patterns were obtained on a STOE STADI P diffractometer equipped with a Dectris Mythen 1K detector (K$_{\alpha 1}$ Cu source, $\lambda = 1.54060$ Å). Luminescence spectra of UCNPs were recorded with an Aminco Bowman Series 2 luminescence spectrometer equipped with an external continuous wave (CW) 980 nm laser module (200 mW) from Picotronic. All luminescence spectra were recorded at room temperature. For lifetime-measurements, an in-house setup consisting of a 980 nm CW laser module (200 mW, ≈15 W cm^{-2}) and an optical chopper was assembled. For the thermogravimetric analysis a Perkin Elmer TGA 7 was used. Fourier-transform infrared spectroscopy measurements were performed by an Agilent Technologies Cary630 FTIR spectrometer.

Surface Modification of Upconversion Nanoparticles Via *NOBF$_4$ Method*: For bioanalytical applications, the surface of oleate-capped UCNPs must be engineered via a two-step ligand exchange method with the assistance of nitrosyl tetrafluoroborate[31] Oleate-capped UCNPs (1 mg) and an equal amount of NOBF$_4$ are added to a two-phase system consisting of equivalent volumes of cyclohexane and *N,N*-dimethylformamide (DMF). The mixture was stirred vigorously for 10 min at 30 °C. Thereby the oleic acid gets protonated and remains in the cyclohexane (upper) phase, whereas the ligand-free UCNPs gets stabilized via BF$_4^-$ in the DMF phase. The cyclohexane phase is discarded. The UCNPs were precipitated from the DMF phase by addition of an excess of chloroform and centrifuged (1000 × g, 5 min). The obtained transparent pellet is washed with chloroform/DMF at least one more time, and then the finally obtained BF$_4^-$ stabilized UCNPs were dispersed in DMF.

For the surface modification with CIT, PAA, PAH, PEG, or PG, the dispersion with the BF$_4^-$ stabilized UCNPs (≈30 mg, 2 mL) was slowly added to a solution of the respective ligand (≈30 mg) in water (2 mL) and stirred for additional 20 min. The particles are collected from the solution by centrifugation (21 000 × g, 30 min) and washed three times to remove the excess of surface ligands. Aggregates are removed by centrifugation (1000 × g, 3 min) and the supernatant is collected and stored in the refrigerator at 4 °C.

Surface Modification of Upconversion Nanoparticles Via *Ligand Removal by HCl*: Oleate capped particles are dried (50 mg) and then dissolved in 5 mL HCl (pH 3, 1×10^{-3} M). The solution was stirred for at least 3 h at 30 °C. Afterward, the remaining oleate was extracted with 5 mL diethyl ether (three times) to remove the free oleic acid molecules. The particles in water were then precipitated with an excess of acetone and centrifuged at 1000 × g for 15 min. The supernatant is discarded. The pellet was redispersed in 5 mL water and stored in the refrigerator at 4 °C.

For the surface modification with PG, the dispersion with the bare UCNPs (≈5 mg mL^{-1}, 1 mL) was slowly added to a solution of the desired ligand (≈5 mg) in water (1 mL) and stirred for additional 30 min. The particles are collected from the solution by centrifugation (21 000 × g, 30 min) and washed three times to remove the excess of the surface ligand. The final dispersion is stored in the refrigerator at 4 °C.

Time-Dependent Colloidal Stability Study and the Influence of Different Solution Systems: UCNPs with different surface coatings (CIT, PEG, PG, PAA, or PAH) were dispersed in dd water at pH 7. Thereby the mass concentration was varied between 5, 1, 0.5, and 0.1 mg mL^{-1}. The particles (1 mL) were filled in a mini dialysis device (Slide-A-Lyzer, MWCO = 10 kDa, total volume of 2 mL) and dialyzed at 37 °C for several hours. At distinct time steps (2.5, 5, 7.5, 10, and 24 h) the solution for dialysis (50 mL) was changed.

Supporting Information

Supporting Information is available from the Wiley Online Library or from the author.

[1] C. Homann, L. Krukewitt, F. Frenzel, B. Grauel, C. Würth, U. Resch-Genger, M. Haase, *Angew. Chem., Int. Ed.* **2018**, *57*, 8765.

[2] T. Cheng, R. Marin, A. Skripka, F. Vetrone, *J. Am. Chem. Soc.* **2018**, *140*, 12890.

[3] S. Wen, J. Zhou, K. Zheng, A. Bednarkiewicz, X. Liu, D. Jin, *Nat. Commun.* **2018**, *9*, 2415.

[4] C. Würth, S. Fischer, B. Grauel, A. P. Alivisatos, U. Resch-Genger, *J. Am. Chem. Soc.* **2018**, *140*, 4922.

[5] B. Tian, A. Fernandez-Bravo, H. Najafiaghdam, N. A. Torquato, M. V. P. Altoe, A. Teitelboim, C. A. Tajon, Y. Tian, N. J. Borys, E. S. Barnard, M. Anwar, E. M. Chan, P. J. Schuck, B. E. Cohen, *Nat. Commun.* **2018**, *9*, 3082.

[6] L. Liang, X. Qin, K. Zheng, X. Liu, *Acc. Chem. Res.* **2019**, *52*, 228.

[7] M. Haase, H. Schäfer, *Angew. Chem., Int. Ed.* **2011**, *50*, 5808.

[8] S. F. Himmelstoß, T. Hirsch, *Methods Appl. Fluoresc.* **2019**, *7*, 22002.

[9] G. A. Mandl, D. R. Cooper, T. Hirsch, J. Seuntjens, J. A. Capobianco, *Methods Appl. Fluoresc.* **2019**, *7*, 12004.

[10] S. Wilhelm, *ACS Nano* **2017**, *11*, 10644.

[11] L. E. Mackenzie, J. A. Goode, A. Vakurov, P. P. Nampi, S. Saha, G. Jose, P. A. Millner, *Sci. Rep.* **2017**, *8*, 1106.

[12] Q. Zou, P. Huang, W. Zheng, W. You, R. Li, D. Tu, J. Xu, X. Chen, *Nanoscale* **2017**, *9*, 6521.

[13] L. Wang, H. Huang, D. Shen, J. Zhang, H. Chen, Y. Wang, X. Liu, D. Tang, *Opt. Express* **2014**, *22*, 19495.

[14] W. Ryba-Romanowski, T. Niedźwiedzki, J. Komar, R. Lisiecki, M. Świrkowicz, *J. Lumin.* **2015**, *162*, 134.

[15] M. W. Pin, E. J. Park, S. Choi, Y. I. Kim, C. H. Jeon, T. H. Ha, Y. H. Kim, *Sci. Rep.* **2018**, *8*, 2199.

[16] T. Rinkel, A. N. Raj, S. Dühnen, M. Haase, *Angew. Chem., Int. Ed.* **2016**, *55*, 1164.

[17] H. T. T. Duong, Y. Chen, S. A. Tawfik, S. Wen, M. Parviz, O. Shimoni, D. Jin, *RSC Adv.* **2018**, *8*, 4842.

[18] V. Muhr, S. Wilhelm, T. Hirsch, O. S. Wolfbeis, *Acc. Chem. Res.* **2014**, *47*, 3481.

[19] M. Buchner, V. Muhr, S. F. Himmelstoß, T. Hirsch, in *Upconverting Nanoparticles* (Ed: C. Altavilla), CRC Press, Boca Raton, FL, USA **2016**, pp. 69–100.

[20] N. Bogdan, F. Vetrone, G. A. Ozin, J. A. Capobianco, *Nano Lett.* **2011**, *11*, 835.

**ADVANCED
SCIENCE NEWS**

www.advancedsciencenews.com

Particle
& Particle Systems Characterization

www.particle-journal.com

[21] R. Naccache, P. Chevallier, J. Lagueux, Y. Gossuin, S. Laurent, L. Vander Elst, C. Chilian, J. A. Capobianco, M.-A. Fortin, *Adv. Healthcare Mater.* **2013**, *2*, 1478.

[22] C. Duan, L. Liang, L. Li, R. Zhang, Z. P. Xu, *J. Mater. Chem. B* **2018**, *6*, 192.

[23] C.-A. J. Lin, R. A. Sperling, J. K. Li, T.-Y. Yang, P.-Y. Li, M. Zanella, W. H. Chang, W. J. Parak, *Small* **2008**, *4*, 334.

[24] O. Dukhno, F. Przybilla, M. Collot, A. Klymchenko, V. Pivovarenko, M. Buchner, V. Muhr, T. Hirsch, Y. Mély, *Nanoscale* **2017**, *9*, 11994.

[25] X. Chen, D. Peng, Q. Ju, F. Wang, *Chem. Soc. Rev.* **2015**, *44*, 1318.

[26] E. L. Rosen, R. Buonsanti, A. Llordes, A. M. Sawvel, D. J. Milliron, B. A. Helms, *Angew. Chem., Int. Ed.* **2012**, *51*, 684.

[27] A. Tsuda, N. K. Venkata, *NanoImpact* **2016**, *2*, 38.

[28] V. Muhr, C. Würth, M. Kraft, M. Buchner, A. J. Baeumner, U. Resch-Genger, T. Hirsch, *Anal. Chem.* **2017**, *89*, 4868.

[29] D. Jaque, L. Martínez Maestro, B. del Rosal, P. Haro-Gonzalez, A. Benayas, J. L. Plaza, E. Martín Rodríguez, J. García Solé, *Nanoscale* **2014**, *6*, 9494.

[30] S. Wilhelm, M. Kaiser, C. Würth, J. Heiland, C. Carrillo-Carrion, V. Muhr, O. S. Wolfbeis, W. J. Parak, U. Resch-Genger, T. Hirsch, *Nanoscale* **2015**, *7*, 1403.

[31] A. Dong, X. Ye, J. Chen, Y. Kang, T. Gordon, J. M. Kikkawa, C. B. Murray, *J. Am. Chem. Soc.* **2011**, *133*, 998.

[32] L. S. Ott, R. G. Finke, *Inorg. Chem.* **2006**, *45*, 8382.

[33] B. Szefczyk, R. Roszak, S. Roszak, *RSC Adv.* **2014**, *4*, 22526.

[34] C. C. Robinson, J. T. Fournier, *Chem. Phys. Lett.* **1969**, *3*, 517.

[35] W. Ren, S. Wen, S. A. Tawfik, Q. P. Su, G. Lin, L. A. Ju, M. J. Ford, H. Ghodke, A. M. van Oijen, D. Jin, *Chem. Sci.* **2018**, *9*, 4352.

[36] W. Kong, T. Sun, B. Chen, X. Chen, F. Ai, X. Zhu, M. Li, W. Zhang, G. Zhu, F. Wang, *Inorg. Chem.* **2017**, *56*, 872.

[37] N. Estebanez, J. Ferrera-González, L. Francés-Soriano, R. Arenal, M. González-Béjar, J. Pérez-Prieto, *Nanoscale* **2018**, *10*, 12297.

[38] N. Estebanez, M. González-Béjar, J. Pérez-Prieto, *ACS Omega* **2019**, *4*, 3012.

[39] A. León, P. Reuquen, C. Garín, R. Segura, P. Vargas, P. Zapata, P. Orihuela, *Appl. Sci.* **2017**, *7*, 49.

[40] H. Li, K. Wang, X. Tuo, L. Almásy, Q. Tian, G. Sun, M. J. Henderson, Q. Li, A. Wacha, J. Courtois, M. Yan, *Mater. Chem. Phys.* **2018**, *204*, 236.

[41] A. Nsubuga, K. Zarschler, M. Sgarzi, B. Graham, H. Stephan, T. Joshi, *Angew. Chem., Int. Ed.* **2018**, *57*, 16036.

[42] M. Xu, M. G. Soliman, X. Sun, B. Pelaz, N. Feliu, W. J. Parak, S. Liu, *ACS Nano* **2018**, *12*, 10104.

[43] J. Hühn J, C. Carrillo-Carrion C, M. G. Soliman MG, C. Pfeiffer, D. Valdeperez, M. Masood, I. Chakraborty, L. Zhu, M. Gallego, Z. Yue, M. Carril, *Chem. Mater.* **2017**, *29*, 399.

[44] M. V. DaCosta, S. Doughan, Y. Han, U. J. Krull, *Anal. Chim. Acta* **2014**, *832*, 1.

[45] F. Wang, X. Liu, *Chem. Soc. Rev.* **2009**, *38*, 976.

[46] J. Chen, J. X. Zhao, *Sensors* **2012**, *12*, 2414.

[47] O. Dukhno, F. Przybilla, V. Muhr, M. Buchner, T. Hirsch, Y. Mély, *Nanoscale* **2018**, *10*, 15904.

[48] D. Lisjak, O. Plohl, J. Vidmar, B. Majaron, M. Ponikvar-Svet, *Langmuir* **2016**, *32*, 8222.

[49] S. Lahtinen, A. Lyytikäinen, H. Päkkilä, E. Hömppi, N. Perälä, M. Lastusaari, T. Soukka, *J. Phys. Chem. C* **2017**, *121*, 656.

[50] S. Han, X. Qin, Z. An, Y. Zhu, L. Liang, Y. Han, W. Huang, X. Liu, *Nat. Commun.* **2016**, *7*, 13059.

[51] J. Xu, Z. Wang, L. Wen, X. Zhou, J, Xu, S. Yang, *Soft Mater* **2016**, *12*, 867.

[52] A. Heuer-Jungemann, N. Feliu, I. Bakaimi, M. Hamaly, A. Alkilany, I. Chakraborty, A. Masood, M. F. Casula, A. Kostopoulou, E. Oh, M. H. Stewart, L. Igor, E. Stratakis, W. J. Parak, A. G. Kanaras, *Chem. Rev.* **2019**, *119*, 4819.

[53] T. Pellegrino, S. Kudera, T. Liedl, A. Munoz Javier, L. Manna, W. J. Parak, *Small* **2019**, *1*, 48.